

# Stabilization and Characterization of a Heme-Oxy Reaction Intermediate in Inducible Nitric-oxide Synthase<sup>\*[5]</sup>

Received for publication, August 7, 2008, and in revised form, September 24, 2008. Published, JBC Papers in Press, September 24, 2008, DOI 10.1074/jbc.M806122200

Jesús Tejero<sup>†1</sup>, Ashis Biswas<sup>‡2</sup>, Zhi-Qiang Wang<sup>‡5</sup>, Richard C. Page<sup>¶</sup>, Mohammad Mahfuzul Haque<sup>‡</sup>, Craig Hemann<sup>||</sup>, Jay L. Zweier<sup>||</sup>, Saurav Misra<sup>¶</sup>, and Dennis J. Stuehr<sup>†3</sup>

From the Departments of <sup>†</sup>Pathobiology and <sup>¶</sup>Molecular Cardiology, The Lerner Research Institute, Cleveland Clinic Foundation, Cleveland, Ohio 44195, the <sup>‡</sup>Department of Chemistry, Kent State University-Tuscarawas, New Philadelphia, Ohio 44663, and the <sup>||</sup>Davis Heart & Lung Research Institute, Division of Cardiovascular Medicine, Department of Internal Medicine, The Ohio State University College of Medicine, Columbus, Ohio 43210

Nitric-oxide synthases (NOS) are heme-thiolate enzymes that *N*-hydroxylate *L*-arginine (*L*-Arg) to make NO. NOS contain a unique Trp residue whose side chain stacks with the heme and hydrogen bonds with the heme thiolate. To understand its importance we substituted His for Trp<sup>188</sup> in the inducible NOS oxygenase domain (iNOSoxy) and characterized enzyme spectral, thermodynamic, structural, kinetic, and catalytic properties. The W188H mutation had relatively small effects on *L*-Arg binding and on enzyme heme-CO and heme-NO absorbance spectra, but increased the heme midpoint potential by 88 mV relative to wild-type iNOSoxy, indicating it decreased heme-thiolate electronegativity. The protein crystal structure showed that the His<sup>188</sup> imidazole still stacked with the heme and was positioned to hydrogen bond with the heme thiolate. Analysis of a single turnover *L*-Arg hydroxylation reaction revealed that a new heme species formed during the reaction. Its build up coincided kinetically with the disappearance of the enzyme heme-dioxy species and with the formation of a tetrahydrobiopterin (H<sub>4</sub>B) radical in the enzyme, whereas its subsequent disappearance coincided with the rate of *L*-Arg hydroxylation and formation of ferric enzyme. We conclude: (i) W188H iNOSoxy stabilizes a heme-oxy species that forms upon reduction of the heme-dioxy species by H<sub>4</sub>B. (ii) The W188H mutation hinders either the processing or reactivity of the heme-oxy species and makes these steps become rate-limiting for *L*-Arg hydroxylation. Thus, the conserved Trp residue in NOS may facilitate formation and/or reactivity of the ultimate hydroxylating species by tuning heme-thiolate electronegativity.

Nitric oxide (NO)<sup>4</sup> plays an essential role in a range of biological processes (1–4). In mammals NO is produced from *L*-Arg by three nitric-oxide synthase (NOS) enzymes (EC 1.14.13.39): neuronal NOS (nNOS), endothelial NOS (eNOS), and inducible NOS (iNOS) (5, 6). All three are comprised of a flavoprotein domain that is linked to a heme-containing oxygenase domain by an intervening calmodulin binding sequence. NOS flavoprotein domains are structurally homologous with cytochrome P450 reductase and related dual-flavin proteins (7–9). In contrast, NOS oxygenase domains (NOSoxy) display a unique structure and fold among heme proteins, bind *L*-Arg and tetrahydrobiopterin (H<sub>4</sub>B) in addition to heme, and interact extensively to form a homodimer (10, 11).

The heme in NOS is bound by cysteine thiolate ligation (10, 11) as occurs in cytochrome P450 enzymes, and this is thought to enable a similar oxygen activation process for the two enzyme families (Fig. 1). However, NOS and cytochrome P450 differ regarding their proximal and distal heme environments (10, 12–15). Some of the distal side differences enable NOS to accommodate its substrate *L*-Arg, whereas the proximal side differences appear to tune the electronic and catalytic properties of the heme. For example, the proximal heme binding loop in NOS enzymes is 1 residue shorter than in cytochrome P450s (supplemental Fig. 1) and contains a conserved tryptophan residue (Trp<sup>409</sup> in rat nNOS, Trp<sup>188</sup> in mouse iNOS) that makes a stacking interaction with the heme and provides a side chain hydrogen bond to the cysteine heme thiolate (supplemental Fig. 1). The homologous residue in the cytochrome P450 superfamily is, with a few exceptions, a phenylalanine that cannot form a hydrogen bond (16), and so the proximal loop peptide backbone contributes all the hydrogen bonds to the cysteine thiolate in cytochrome P450 (17) (supplemental Fig. 1).

Hydrogen bonding to the cysteine thiolate is thought to impact heme reactivity in cytochrome P450 enzymes (18). Likewise, we previously reported that removal of the hydrogen bond provided by Trp<sup>409</sup> in nNOS significantly altered the properties

\* This work was supported, in whole or in part, by National Institutes of Health Grants CA53914, GM51491, HL76491 (to D. J. S.), GM080271 (to S. M.), HL63744, HL65608, and HL38324 (to J. L. Z.). This work was also supported by American Heart Association Beginning Grant-in-Aid 0565297B (to Z.-Q. W.). The costs of publication of this article were defrayed in part by the payment of page charges. This article must therefore be hereby marked "advertisement" in accordance with 18 U.S.C. Section 1734 solely to indicate this fact.

[5] The on-line version of this article (available at <http://www.jbc.org>) contains supplemental Figs. S1–S4 and Tables S1 and S2.

The atomic coordinates and structure factors (code 3DWJ) have been deposited in the Protein Data Bank, Research Collaboratory for Structural Bioinformatics, Rutgers University, New Brunswick, NJ (<http://www.rcsb.org/>).

<sup>1</sup> Supported by American Heart Association Postdoctoral Fellowship 0625632B.

<sup>2</sup> Supported by American Heart Association Postdoctoral Fellowship 0825545D.

<sup>3</sup> To whom correspondence should be addressed: Lerner Research Institute (NC-22), The Cleveland Clinic Foundation, 9500 Euclid Ave., Cleveland, OH 44195. Tel.: 216-445-6950; Fax: 216-636-0104; E-mail: [stuehrd@ccf.org](mailto:stuehrd@ccf.org).

<sup>4</sup> The abbreviations used are: NO, nitric oxide; Cpd I, compound I; Cpd II, compound II; EPPS, 4-(2-hydroxyethyl)-1-piperazinepropanesulfonic acid; H<sub>2</sub>B, 7,8-dihydro-L-biopterin; H<sub>4</sub>B, (6R)-5,6,7,8-tetrahydro-L-biopterin; *L*-Arg, *L*-arginine; NADPH, nicotinamide adenine dinucleotide phosphate, reduced form; NOHA, N<sup>ω</sup>-hydroxyl-L-arginine; NOS, nitric-oxide synthase; eNOS, endothelial nitric-oxide synthase; iNOS, inducible nitric-oxide synthase; iNOSoxy, oxygenase domain of the inducible nitric-oxide synthase; nNOS, neuronal nitric-oxide synthase; WT, wild-type; HPLC, high pressure liquid chromatography; MES, 4-morpholineethanesulfonic acid.

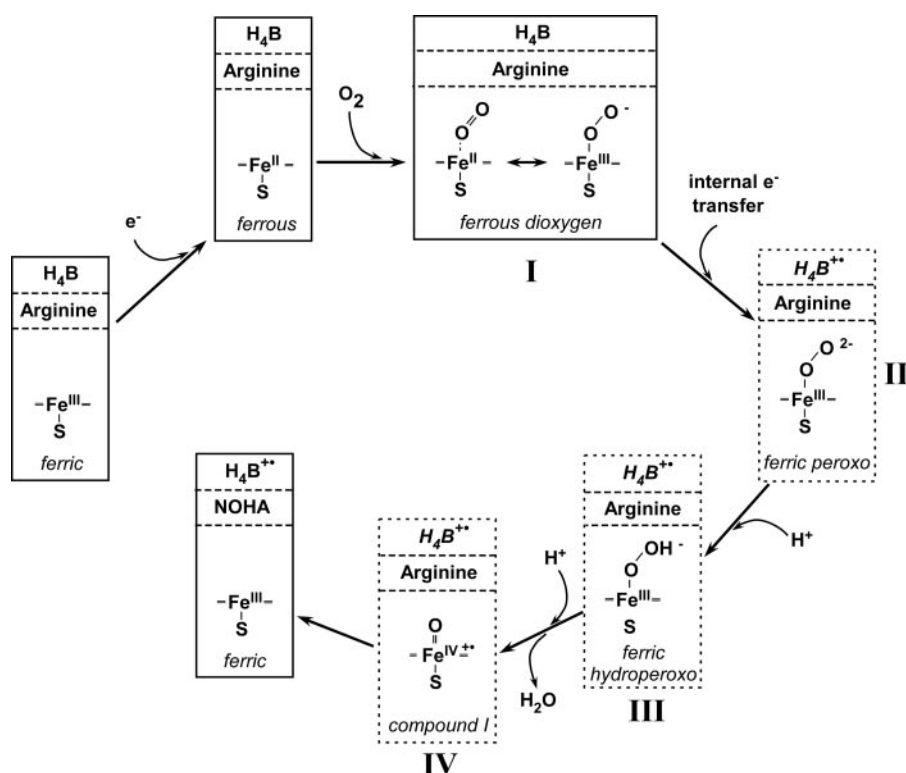


FIGURE 1. Reaction scheme for the single turnover L-Arg hydroxylation of NOS enzymes. After formation of the ferrous dioxygen complex (I) the subsequent steps are fast and none of the three putative intermediates (II, III, and IV; dashed boxes) have been spectroscopically observed in single turnover reactions. See text for details.

and reactivity of its heme, as judged by results obtained with the W409F nNOS mutant (19–21). More recently, we mutated the analogous Trp<sup>188</sup> residue in iNOSoxy to histidine (W188H). As described herein, we found that W188H iNOSoxy stabilizes an enzyme reaction intermediate during L-Arg hydroxylation that forms downstream from the ferrous-dioxy species (I in Fig. 1) and normally does not build up in wild-type enzyme. Further characterization of W188H iNOSoxy suggests how specific changes in heme-thiolate electronic properties may stabilize heme-oxy intermediates in heme-thiolate enzymes.

## EXPERIMENTAL PROCEDURES

**Chemicals**—H<sub>4</sub>B and H<sub>2</sub>B were purchased from Schircks Laboratories (Jona, Switzerland). Other reagents were purchased from sources previously reported (21–23).

**Mutagenesis**—Site-directed mutagenesis of the mouse Δ65 iNOSoxy domain (amino acids 66 to 498) and the Δ65 iNOS full-length (amino acids 66 to 1144) were performed using the QuikChange XL Site-directed mutagenesis kit (Stratagene, La Jolla, CA). Mutations were introduced with the primers: W188H forward, 5'-CAA GAT GGC CCA TAG GAA TGC CCC TCG CTG CAT CGG CAG AAT CCA GTG GTC-3'; W188H reverse, 5'-GAC CAC TGG ATT CTG CCG ATG CAG CGA GGG GCA TTC CTA TGG GCC ATC TTG-3', the mutation sites are underlined. Mutations were confirmed by DNA sequencing at the Cleveland Clinic Genomics Core Facility. Mutated plasmids were transformed into BL21(DE3) *Escherichia coli* cells using the TransformAid bacterial transformation kit (Fermentas, Hanover, MD).

**Protein Expression and Purification**—The Δ65iNOSoxy W188H mutant with a His<sub>6</sub> tag at the C terminus was overexpressed in *E. coli* strain BL21(DE3) using a modified pCWori vector. The protein was purified in the presence of H<sub>4</sub>B and L-Arg as previously described (24). The modified pCWori vector encoding the Δ65iNOS full-length W188H mutant with an N-terminal His<sub>6</sub> tag was transformed into *E. coli* BL21(DE3) cells carrying the pACYC plasmid encoding human Calmodulin. The full-length protein was overexpressed and purified as described (25). Protein concentration was determined from the absorbance at 444 nm of the ferrous heme-CO complex, using an extinction coefficient of 74 mM<sup>-1</sup> cm<sup>-1</sup> (Δε<sub>444–500 nm</sub>) (26). UV-visible spectra of ferric, ferrous enzyme, and complexes were recorded in either a Cary 100 or a Shimadzu UV-2401 PC spectrophotometer.

**Redox Potentiometry**—Redox titrations were carried out in a glove box (Belle Technology, Dorset, UK)

under nitrogen atmosphere as previously described (23, 27). Protein sample (final concentration ≈10 μM) was made anaerobic by gel filtration in a Sephadex G-25 column (PD10, GE Healthcare) equilibrated with anaerobic buffer (potassium phosphate, 0.1 M, pH 7.0, 125 mM NaCl). After elution, the samples were diluted to a 7-ml final volume and H<sub>4</sub>B (25 μM) and L-Arg (2.5 mM) was added. Measurements were carried out at 15 ± 1 °C. Absorption spectra were recorded in Cary 50 using a dip probe detector, and the potentials were monitored using an Accumet AB15 (Fisher Scientific) coupled to a silver/silver chloride electrode saturated with 4 M KCl. Redox mediators (Sigma) 1–5 μM anthraquinone-2-sulfonate (*E*<sub>m</sub> –225 mV), phenosafranin (*E*<sub>m</sub> –252 mV), and benzyl viologen (*E*<sub>m</sub> –358 mV) (*E*<sub>m</sub>, midpoint redox potential) were used. A correction factor of +209 mV at 15 °C was used as previously determined (27). The one electron midpoint potentials were determined from the difference spectra. Fractions oxidized for each spectra were calculated from the maximum difference between oxidized and reduced spectra (around 430 and 390 nm). Using these data and the corresponding measured potentials (*versus* SHE) the midpoint potential of the half-reaction can be determined using the Nernst equation (Equation 1),

$$E = E_m + \frac{RT}{nF} 2.303 \log \frac{[\text{Oxidized}]}{[\text{Reduced}]} \quad (\text{Eq. 1})$$

where *E* is the measured equilibrium potential at each titration point, *R* is the gas constant (8.314 J·mol<sup>-1</sup> K<sup>-1</sup>), *T* is the experimental temperature in Kelvin, *n* is the number of elec-

## Stabilization of a Reaction Intermediate in iNOS

trons in the half-reaction,  $F$  is the Faraday constant (96,485 C/mol), and [Oxidized]/[Reduced] is the ratio of oxidized to reduced species.

**Crystal Growth, Data Collection, and Structure Refinement**—Crystals of murine W188H-iNOS $\Delta$ 65 (residues 66–498) were grown at 4 °C using the hanging drop method as described in Ref. 10 with some minor modifications. The W188H iNOS $\Delta$ 65 concentration was 18–20 mg/ml in 40 mM EPPS (pH 7.6) containing 10% glycerol, 50 mM NaCl, 10 mM H<sub>4</sub>B, and 10 mM L-Arg. The reservoir contained 0.46–0.74 M Li<sub>2</sub>SO<sub>4</sub>, 100 mM MES (pH 4.9–5.9), and 5%  $\beta$ -octyl glucoside. 1.0  $\mu$ l of protein was mixed with an equal volume of reservoir solution and crystals were grown in 5–8 days. Instead of Li<sub>2</sub>SO<sub>4</sub>, we used 0.7–1.2 M (NH<sub>4</sub>)<sub>2</sub>SO<sub>4</sub> in the reservoir solution and we found that crystals were grown in 3–6 days. Crystals were frozen using 30% ethylene glycol as cryoprotectant. Several iNOS W188H crystal data sets were collected at Advanced Light Source beamline 4.2.2, Lawrence Berkeley National Laboratory. Diffraction data were indexed, integrated, and scaled using d\*TREK (28). All crystals tested were in space group P6<sub>1</sub>22. Although the crystals exhibited highly anisotropic diffraction, one crystal diffracted with reasonable completeness to 2.75-Å resolution. The structure of the wild-type iNOS oxygenase  $\Delta$ 65-fragment (RCSB code 1NOD (10)) was used as a starting model for molecular replacement in PHASER (29). Density map interpretation and model rebuilding were carried out using COOT (30). Refinement was carried out in PHENIX (31) to generate a final model with an  $R$ -factor of 22.3% and a free  $R$ -factor of 29.4%. The refined structure has no Ramachandran violations. Crystallographic data collection and refinement statistics are summarized in supplemental Table 2.

**L-Arg and Imidazole Binding**—L-Arg and imidazole binding affinity was studied at 25 °C by difference spectroscopy (32). iNOS samples (around 5  $\mu$ M) in 40 mM EPPS buffer (pH 7.6) with 10% glycerol, and 100  $\mu$ M H<sub>4</sub>B were titrated with either L-Arg or imidazole (final concentration 400–800  $\mu$ M). The  $K_d$  of L-Arg was calculated by fitting of the absorbance difference versus the substrate concentration.

**Single Turnover Reactions**—L-Arg hydroxylation experiments were carried out in a Hi-Tech SF61-DX2 stopped-flow instrument (Hi-Tech Scientific, Salisbury, UK) coupled to a diode array detector, as previously described (33). The reaction was studied in the presence of 50  $\mu$ M H<sub>4</sub>B or 100  $\mu$ M H<sub>2</sub>B, 1 mM L-Arg, 150 mM NaCl, 10% glycerol, 1 mM dithiothreitol in 40 mM EPPS buffer (pH 7.6). 10  $\mu$ M iNOS $\Delta$ 65 was titrated with sodium dithionite and mixed with air-saturated buffer at room temperature ([O<sub>2</sub>]  $\approx$  280  $\mu$ M). Sequential spectral data were fitted to A  $\rightarrow$  B  $\rightarrow$  C and A  $\rightarrow$  B  $\rightarrow$  C  $\rightarrow$  D models using the Specfit/32 global analysis software, version 3.0 (Spectrum Software Associates, Marlborough, MA), which calculates the spectra of the different enzyme species and their concentration change versus time.

**Rapid-freeze Kinetic Experiments**—Ferrous iNOS samples prepared by titrating ferric protein solutions with sodium dithionite as described above were transferred with an anaerobic syringe to a rapid quench instrument (RQF-63, Hi-Tech Scientific, Salisbury, UK) maintained at 10 °C and the samples were rapidly mixed with an O<sub>2</sub>-saturated buffer (40 mM EPPS,

125 mM NaCl, pH 7.5) to initiate the reaction. The reaction mixture was then aged for various times in the instrument followed by rapid injection into a liquid N<sub>2</sub>/isopentane freezing solution as described elsewhere (34, 35).

**Electron Paramagnetic Resonance**—EPR spectra were recorded on a Bruker ESP 300E electron paramagnetic resonance (EPR) spectrometer equipped with an EIP Model 28B microwave frequency counter. All spectra were obtained at 150 K using a microwave power of 2 milliwatts, microwave frequency of 9.45 GHz, modulation amplitude of 5.0 G, and modulation frequency of 100 kHz. Ten scans per sample were accumulated to improve signal to noise ratio, and spin quantitations were calculated by double integration.

**Rapid-quench Experiments**—We performed these experiments as previously described (34) with some modifications. Briefly, an anaerobic solution of 100  $\mu$ M ferrous wild-type iNOS $\Delta$ 65, 130  $\mu$ M L-Arg, 0.5 mM H<sub>4</sub>B, and 0.1 mM dithiothreitol in 40 mM EPPS, 10% glycerol, 150 mM NaCl (pH 7.6) was mixed at 10 °C with a syringe containing oxygen-saturated 40 mM EPPS, 10% glycerol, 150 mM NaCl (pH 7.6), and 150  $\mu$ M L-Arg. The quenching solution was 1.0 N HCl, in all cases. For W188H iNOS $\Delta$ 65 the protein and L-Arg concentrations were 150 and 200  $\mu$ M, respectively. Quenched reaction samples were collected and stored at –70 °C. To determine the final dilution factors the protein samples included 200  $\mu$ M L-glutamic acid as an internal standard.

**Determination of Reaction Products by HPLC**—L-Arg, NOHA, and citrulline in the rapid-quench samples were derivatized with *o*-phthalaldehyde and quantified by HPLC as described previously (36, 37). A complete procedure is provided under supplementary materials.

**Stoichiometry of L-Arg Hydroxylation**—A solution containing 1 mM wild-type iNOS $\Delta$ 65 or W188H, 3 mM L-Arg, 1.0 mM H<sub>4</sub>B, 0.5 mM dithiothreitol, 10% glycerol, 150 mM NaCl in 40 mM EPPS buffer (pH 7.6) was made anaerobic and titrated with sodium dithionite to produce the ferrous enzyme. Different amounts of these stock solutions were mixed with air-saturated buffer containing 3 mM L-Arg, 10% glycerol, 150 mM NaCl in 40 mM EPPS (pH 7.6) at room temperature. For completion of the reaction, these solution mixtures were incubated for 10 min. The reaction was quenched by adding 5  $\mu$ l of 1.0 N HCl to the reaction mixtures (total volume 100  $\mu$ l) and the samples were stored at –70 °C. NOHA formed in these samples were estimated using the above described HPLC method.

**Steady-state Assays**—NO synthesis and NADPH oxidation rates were determined using the oxyhemoglobin assay (22). The NO synthesis activity was determined by the conversion of oxyhemoglobin to methemoglobin using an extinction coefficient of 38 mm<sup>-1</sup> cm<sup>-1</sup> at 401 nm. The NADPH oxidation rates were determined following the absorbance at 340 nm, using an extinction coefficient of 6.2 mm<sup>-1</sup> cm<sup>-1</sup>. Reaction mixtures (total volume 400  $\mu$ l) contained  $\leq$ 0.2  $\mu$ M iNOS, 0.3 mM dithiothreitol, 4  $\mu$ M FAD, 4  $\mu$ M FMN, 4  $\mu$ M H<sub>4</sub>B, 10 mM L-Arg, 0.1 mg/ml bovine serum albumin, 0.8 mM CaCl<sub>2</sub>, 0.2 mM EDTA, 1  $\mu$ M calmodulin, 100 units/ml catalase, 60 units/ml superoxide dismutase, 5  $\mu$ M oxyhemoglobin, and 150 mM NaCl in 40 mM EPPS buffer (pH 7.6). The reaction was initiated by adding

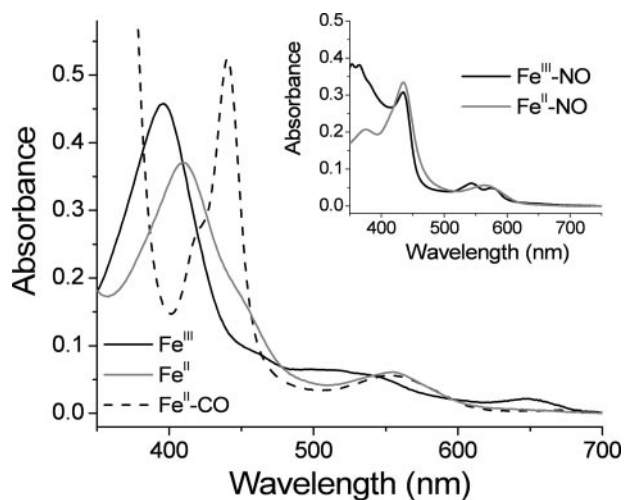


FIGURE 2. Spectral properties of the W188H iNOSoxy mutant in the presence of  $H_4B$  and L-Arg. Representative spectra for the enzyme in the oxidized and reduced states, as well as the  $Fe^{II}$ -CO,  $Fe^{II}$ -NO, and  $Fe^{III}$ -NO complexes are shown.

NADPH to a final concentration of  $250 \mu M$ . All steady-state assays were carried out at  $25^\circ C$ .

## RESULTS

**Protein Expression, Spectroscopic Properties, and Substrate Binding**—The expression level of W188H iNOSoxy was similar to wild-type and the mutant contained bound heme, which is remarkable because another substitution at this site in iNOSoxy (W188F) was reported to generate a predominantly heme-free protein (38). UV-visible spectra of W188H iNOSoxy are shown in Fig. 2. In the absence of  $H_4B$  and L-Arg the mutant enzyme had a 417-nm Soret band, indicating a low-spin ferric heme. Addition of  $H_4B$  and L-Arg shifted the Soret maximum to 396 nm, indicating a predominant high-spin character as occurs in wild-type iNOSoxy (39). Spectra of the  $Fe^{II}$ -CO,  $Fe^{II}$ -NO, and  $Fe^{III}$ -NO complexes of W188H iNOSoxy are similar but not identical to wild-type (Fig. 2 and Table S1). The  $K_d$  for L-Arg in W188H iNOSoxy was determined using a spectroscopic assay to be  $29 \pm 3 \mu M$ , which is roughly 20 times greater than the wild-type  $K_d$  value of  $1.3 \pm 0.9 \mu M$  determined under identical conditions. Together, this indicates that the heme-thiolate ligation is intact in W188H iNOSoxy, but its heme electronic environment and substrate binding affinity have some detectable differences compared with wild-type.

**Crystal Structure of W188H iNOSoxy**—We obtained a crystal structure of W188H iNOSoxy at 2.8-Å resolution. Parameters are reported in supplemental Table S2. Overall, the structure of the mutant is highly similar to wild-type iNOSoxy. Fig. 3 focuses on the heme structural environments of W188H and wild-type iNOSoxy. In the mutant, the His<sup>188</sup> imidazole side chain is positioned below the heme and in the space that is normally occupied by the Trp<sup>188</sup> side chain in native iNOSoxy. The imidazole ring of His<sup>188</sup> makes a stacking interaction with the porphyrin ring, and its N<sup>ϵ</sup> atom is positioned within a similar H-bonding distance to the heme thiolate as is the indole nitrogen of Trp<sup>188</sup> in wild-type iNOSoxy. The porphyrin ring appears to be bent in a similar manner in both mutant and wild-type structures, although the iron atom appears to lie

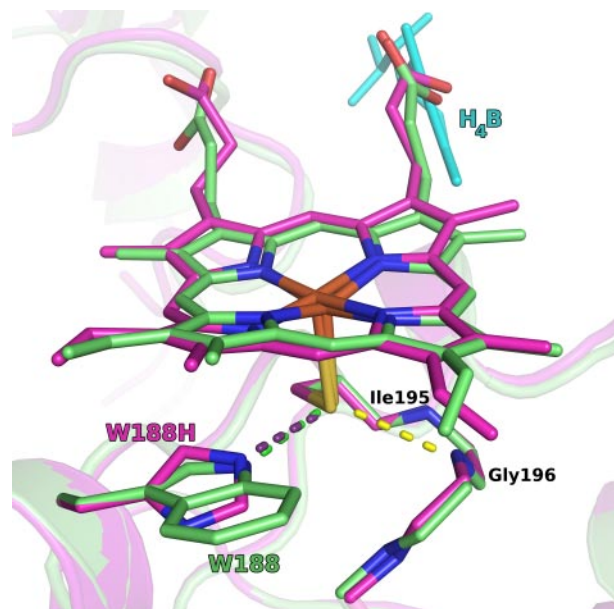


FIGURE 3. Comparison of wild-type and W188H mutant iNOSoxy. Structures of wild-type (green, PDB 1NOD (10)) and W188H iNOSoxy (magenta) exhibit similar structures in the heme region. The orientation of the wild-type Trp<sup>188</sup> indole nitrogen and W188H  $\epsilon$  nitrogen are consistent and both point toward the Cys<sup>194</sup> sulfide. Hydrogen bonds are shown between the Cys<sup>194</sup> sulfide and the Trp<sup>188</sup> indole nitrogen (magenta dashes), between the Cys<sup>194</sup> sulfide and the His<sup>188</sup>  $\epsilon$  nitrogen (green dashes), and between Cys<sup>194</sup> sulfide and Gly<sup>196</sup> backbone nitrogen (yellow dashes) are marked. The peptidic nitrogen of Ile<sup>195</sup> is not in a proper geometry for a hydrogen bond with the sulfide but the partial positive charges of the N-H hydrogen may contribute electrostatic interactions with the thiolate. Throughout the figure nitrogen (blue) and oxygen (red) are colored separately for clarity. The  $H_4B$  molecule from the W188H structure is shown in cyan, the other  $H_4B$  molecule is omitted for clarity. The figure was generated using PyMOL (96).

more in-plane with the porphyrin ring in the mutant enzyme. These structural features are consistent with our biochemical/biophysical measurements on W188H iNOSoxy.

**Redox Potentiometry**—One possible impact of the W188H mutation is an effect on the heme midpoint potential. We therefore compared the ferric/ferrous heme midpoint potentials of our W188H and wild-type iNOSoxy proteins in the presence of  $H_4B$  and L-Arg. Data from representative spectroelectrochemical titrations are shown in Fig. 4. The calculated  $E_m$  value for the wild-type iNOSoxy was  $-261 \pm 2$  mV, in good agreement with previous values ( $-263$  mV (40) and  $-270$  mV (41)) obtained at  $25^\circ C$ . The W188H mutant had a heme midpoint potential of  $-173 \pm 2$  mV, which is an +88 mV increase over wild type. Thus, substituting His for Trp<sup>188</sup> in iNOSoxy caused a significant increase in the ferric/ferrous heme midpoint potential.

**Stopped-flow Analysis of a Single Turnover L-Arg Hydroxylation**—We next studied heme transitions that occur in W188H iNOSoxy during catalysis of Arg hydroxylation under single turnover conditions. The W188H iNOSoxy protein was saturated with L-Arg and  $H_4B$ , reduced with dithionite under anaerobic conditions, and then mixed in a stopped-flow instrument with air-saturated buffer containing L-Arg and  $H_4B$  to start the reaction. Replica reactions with wild-type iNOSoxy were run for comparison. Diode array spectra were collected over the course of each reaction, and subject to global analysis. We found the L-Arg hydroxylation reaction of W188H

## Stabilization of a Reaction Intermediate in iNOS

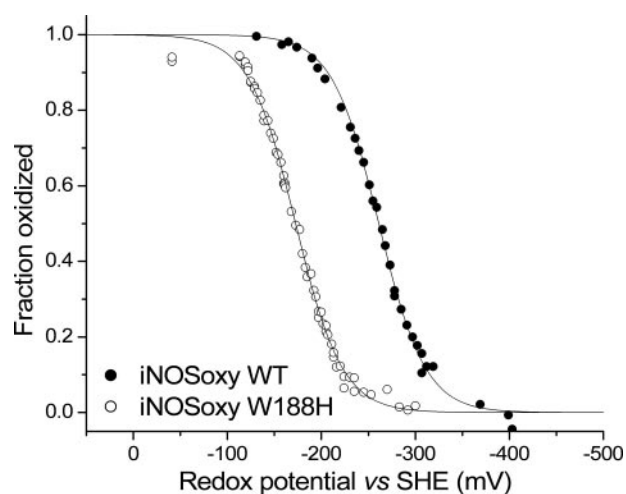


FIGURE 4. **Determination of the redox potential of wild-type and W188H iNOSoxy proteins.** The fraction of oxidized protein at each redox potential value was fitted to the Nernst equation. The fitted values are: iNOSwt,  $-261 \pm 2$  mV; W188H,  $-173 \pm 2$  mV.

iNOSoxy to be more complex than that of wild-type iNOSoxy. A three-species, two consecutive transition model that typically provides a good fit for the wild-type reaction (34) (Equation 2),



led to considerable error in the case of W188H iNOSoxy. However, a four-species, three consecutive transition model that includes formation of a new intermediate after the heme-dioxy species could achieve an accurate fit (Equation 3).



Visual analysis of the collected spectral scans confirmed the appearance of a new intermediate at this point in the reaction (data not shown). The calculated spectrum of each W188H iNOSoxy heme species, and the time courses of their formation and/or disappearance during the Arg hydroxylation reaction, are shown in Fig. 5. The calculated transition rates are summarized in Table 1 and compared with rates we obtained in a wild-type iNOSoxy reaction. The formation rate of the heme-dioxy complex was relatively fast and was similar for either protein. Formation of the new heme intermediate in W188H iNOSoxy coincided with the disappearance of its heme dioxy complex (species I in Fig. 1). Buildup of the new intermediate implies that the W188H mutation stabilizes a heme-oxy species that forms downstream from the heme-dioxy species but normally does not build up during the L-Arg hydroxylation reaction catalyzed by iNOSoxy (34).

**Requirement for  $\text{H}_4\text{B}$** —The NOS heme-dioxy complex (species I in Fig. 1) must receive an electron from bound  $\text{H}_4\text{B}$  (42) for NOS to form downstream heme-oxy species that can hydroxylate L-Arg (Fig. 1). We therefore tested if the new heme-oxy species we observed in the W188H iNOSoxy reaction would still form if the reaction was run using a W188H iNOSoxy protein that contained the redox-inactive dihydrobiopterin ( $\text{H}_2\text{B}$ ) in place of  $\text{H}_4\text{B}$  (Fig. S3). In this case, the  $\text{Fe}^{\text{II}}\text{O}_2$  complex still formed but then transformed slowly ( $0.0044 \text{ s}^{-1}$ )

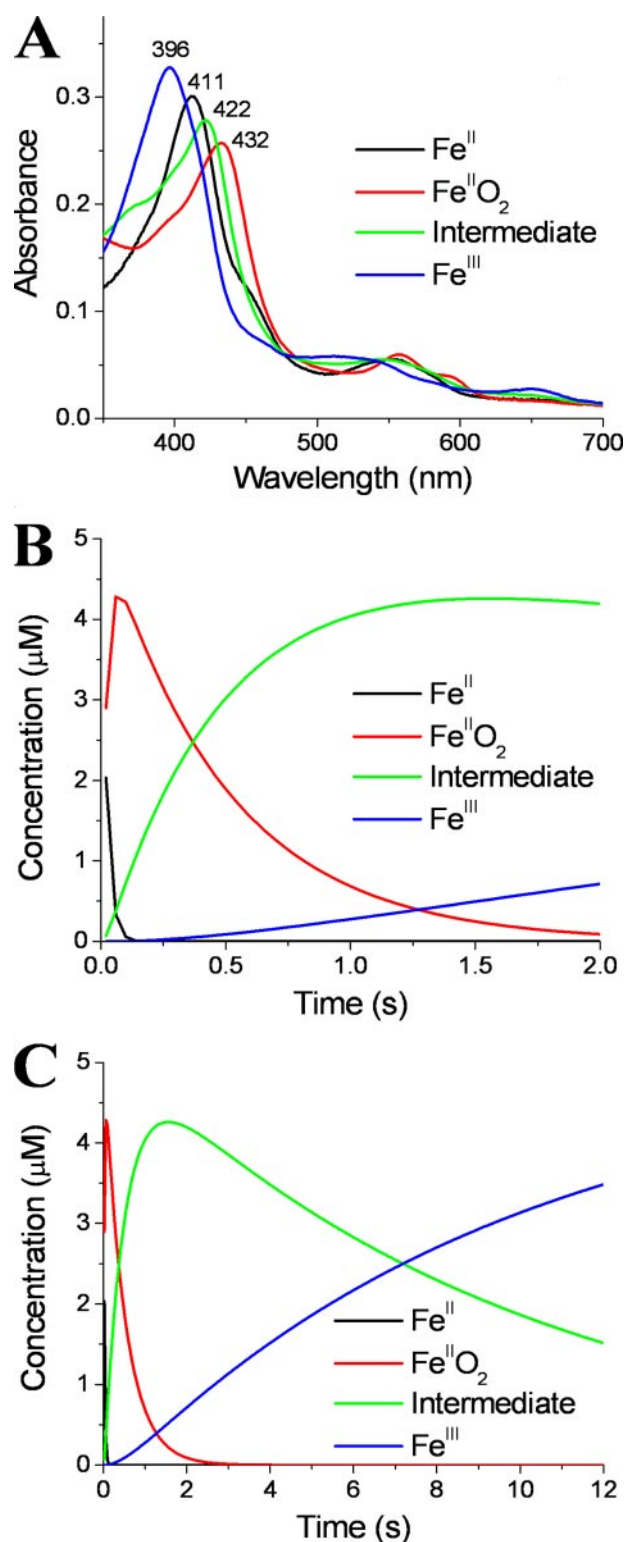
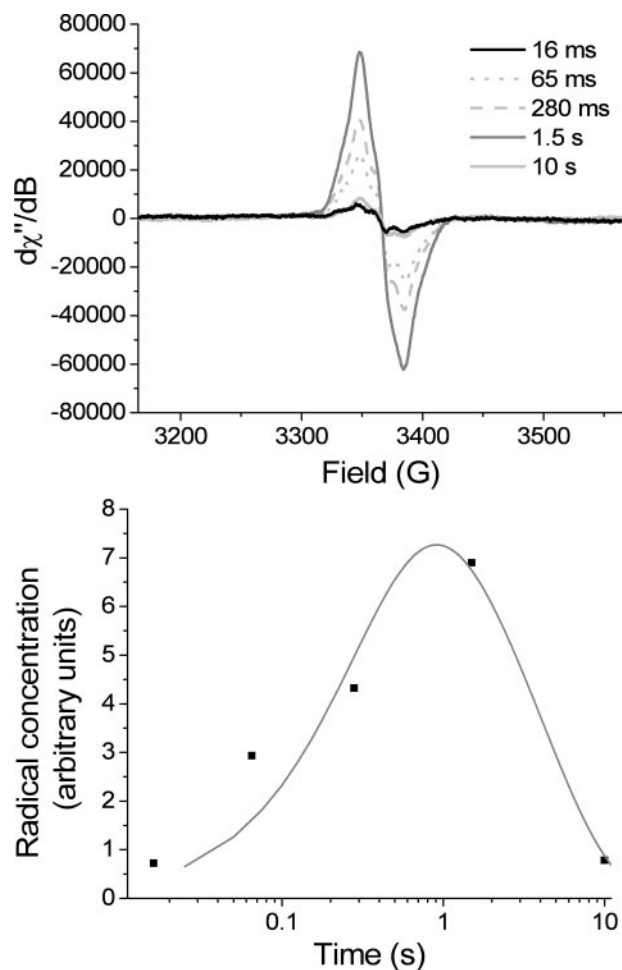


FIGURE 5. **Stopped-flow analysis of the heme transitions during L-Arg hydroxylation by the W188H iNOSoxy mutant.** Single turnover reactions were initiated by mixing anaerobic ferrous protein with air saturated buffer at  $10^\circ\text{C}$ . A, spectra of the  $\text{Fe}^{\text{II}}$ ,  $\text{Fe}^{\text{II}}\text{O}_2$ , Intermediate, and  $\text{Fe}^{\text{III}}$  heme species as calculated from Specfit global analysis of the kinetic data. The wavelength of the Soret band peaks is indicated. B and C, concentration of the  $\text{Fe}^{\text{II}}$ ,  $\text{Fe}^{\text{II}}\text{O}_2$ , Intermediate, and  $\text{Fe}^{\text{III}}$  heme species versus time during the short (B) or longer times (C) as calculated from Specfit global analysis of the kinetic data.

**TABLE 1**  
Observed rate constants for heme transitions during the single turnover experiments with L-Arg

Enzyme	Observed transition rates ( $s^{-1}$ )		
	$Fe^{II} \rightarrow Fe^{II}O_2 \rightarrow Fe^{III}$		
iNOSoxy wt <sup>a</sup>	$52.7 \pm 2.2$		$12.5 \pm 0.2$
	$Fe^{II} \rightarrow Fe^{II}O_2 \rightarrow Int \rightarrow Fe^{III}$		
iNOSoxy W188H	$46.0 \pm 1.1$	$2.03 \pm 0.04$	$0.104 \pm 0.003$

<sup>a</sup> Data from Ref. 34.



**FIGURE 6. Formation of the  $H_4B$  radical in the W188H iNOSoxy single turnover reaction at 10 °C as monitored by EPR.** Top, spectra at different time points. Bottom, fit of the radical concentration to B according to an  $A \rightarrow B \rightarrow C$  reaction scheme.

into ferric enzyme without formation of the new intermediate. Kinetically, the behavior of the  $H_2B$ -bound W188H iNOSoxy was similar to that described for  $H_2B$ -bound wild-type iNOSoxy (33), whose ferrous-dioxy transformation to ferric enzyme is also slow ( $0.3 s^{-1}$  under identical conditions). We conclude that W188H iNOSoxy requires  $H_4B$  to form the new heme-oxy reaction intermediate.

The above result implies that formation of the new heme-oxy species may depend on electron transfer from  $H_4B$ . We verified this directly by detecting formation of an  $H_4B$  radical in the single turnover L-Arg hydroxylation reaction catalyzed by W188H iNOSoxy. Fig. 6 contains EPR spectra of reaction samples that were frozen at various times after initiating the reaction. There was a significant  $H_4B$  radical formation with an

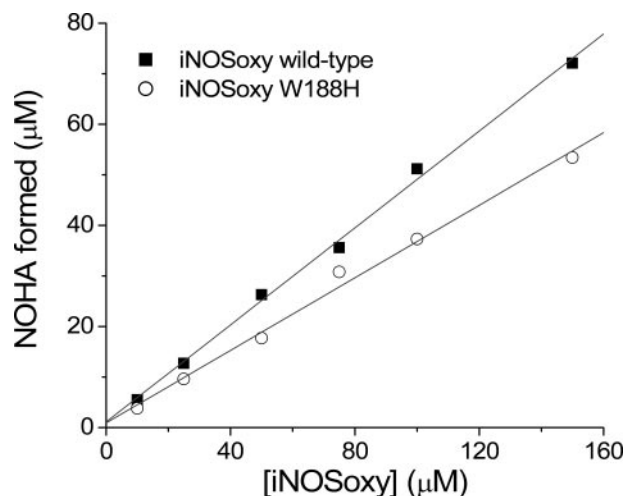


**FIGURE 7. Stoichiometry of NOHA formation by wild-type and W188H iNOSoxy in the single turnover reaction.** Samples of wild-type or W188H iNOSoxy were prereduced with a stoichiometric amount of dithionite and then mixed with aerobic buffer and incubated for 10 min (see text for details). The amount of NOHA formed from different starting concentrations of NOS was quantified by HPLC.

estimated rate<sup>5</sup> of  $3.0 \pm 1.4 s^{-1}$ . At the early and late time points, the shape of the radical spectrum was very similar to that observed for the  $H_4B$  radical in wild-type iNOSoxy reactions (34). However, in one intermediate sample (1.5 s, Fig. 6), the EPR spectrum appeared to include an additional  $G = 2.0$  radical signal, which we estimate represents about 40 to 50% of the total radical signal present at this time point (Fig. S4). The nature of this new radical is currently under investigation.

Together, our data indicate that  $H_4B$  radical formation in W188H iNOSoxy is coincident with conversion of the heme-dioxy complex I to the new heme-oxy intermediate that builds up in our stopped-flow experiment ( $k_{obs} = 2.0 s^{-1}$ , Table 1). Thus, the new intermediate appears to form as a consequence of heme-dioxy reduction by  $H_4B$ .

**Extent and Kinetics of L-Arg Hydroxylation**—To determine whether the new heme-oxy intermediate was a catalytically competent species, we measured the extent and kinetics of NOHA formation in single turnover L-Arg hydroxylation reactions that were catalyzed by W188H or wild-type iNOSoxy. As shown in Fig. 7, the two proteins generated comparable amounts of NOHA (an average of 0.37 and 0.49 per heme, respectively) in the single turnover reactions. These efficiencies of product formation are within the range found in the literature for wild-type iNOSoxy (0.4 to 0.8 NOHA per heme) (34, 37, 43, 44). We next measured the kinetics of NOHA formation using a rapid-quench technique and HPLC analysis (34, 37). The time course of the L-Arg hydroxylation is shown in Fig. 8. The W188H mutant catalyzed the conversion of L-Arg at a much slower rate than wild-type enzyme. The rates of L-Arg disappearance and NOHA formation by W188H iNOSoxy were similar and could be fit to a single exponential equation,

<sup>5</sup> Rates are only estimates, as the main focus of the experiment was to confirm  $H_4B$  radical formation and not to determine rates. Furthermore, the possible appearance of other radical signals in addition to the  $H_4B$  radical may be significant and bias the double integration values. These issues will require further analysis.

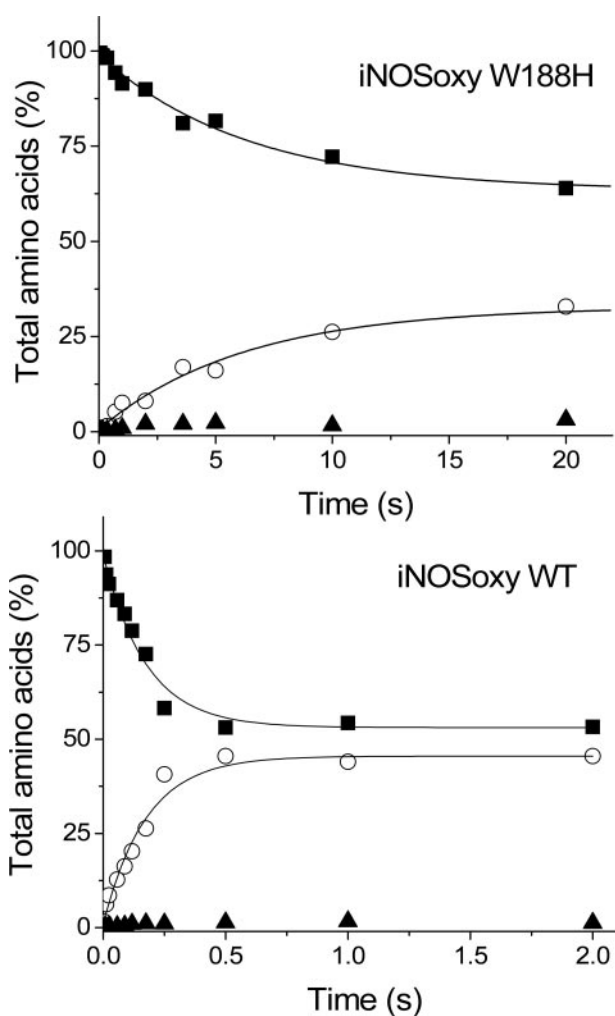


FIGURE 8. Kinetics of product formation as determined by rapid-quench experiments and HPLC analysis. Anaerobic ferrous W188H was mixed with oxygen saturated buffer at 10 °C. Samples were quenched at different times and the concentrations of L-Arg (closed squares), NOHA (open circles), and citrulline (closed triangles) were determined by HPLC. Lines indicate the fit to a single exponential equation.

giving a rate of  $0.159 \text{ s}^{-1}$ . Significantly, this rate of product formation is comparable with the conversion rate of the new heme-oxy intermediate in our stopped-flow experiments ( $0.104 \text{ s}^{-1}$ , Table 1). This implies the new heme-oxy intermediate is a catalytically competent species.

**NO Synthesis**—The steady-state NO synthesis rate of the full-length iNOS W188H enzyme was determined by the oxyhemoglobin NO capture assay. The observed rates were  $6.4 \text{ min}^{-1}$  (NO synthesis) and  $50 \text{ min}^{-1}$  (NADPH oxidation), significantly lower than the values observed for the wild-type enzyme under the same conditions (NO synthesis,  $66 \text{ min}^{-1}$ ; NADPH oxidation,  $116 \text{ min}^{-1}$ ). NO synthesis is thus slower in the mutant, with more uncoupled NADPH consumption.

## DISCUSSION

L-Arg hydroxylation is the first reaction that NOS catalyzes during NO synthesis. As in cytochrome P450 systems (17, 45–49), the reaction is thought to involve stepwise  $\text{O}_2$  activation at the heme (Fig. 1) to ultimately generate a Cpd I-like species that inserts an oxygen atom into a  $\text{N}^{\omega}$ -H bond of L-Arg

(5, 50, 51) (Fig. 1). The initial heme-dioxy species that forms when  $\text{O}_2$  binds to ferrous heme is well characterized in NOS, and there is much information available on its spectroscopic properties, formation, and decay kinetics, and lack of reactivity toward L-Arg or NOHA (34, 37, 43, 52–58). However, once the heme-dioxy species forms, its subsequent reduction by  $\text{H}_4\text{B}$  becomes rate-limiting for further catalysis (34, 59). This prevents accumulation of downstream reactive heme-oxy species during L-Arg hydroxylation, and one instead observes monophasic conversion of the heme-dioxy species to the ferric enzyme during a single turnover reaction (52). Here we observed build up of a new heme-oxy intermediate in W188H iNOSoXy during its L-Arg hydroxylation. Our time-resolved UV-visible and EPR data indicate that this new intermediate forms downstream from the initial heme-dioxy species and forms as a consequence of heme-dioxy reduction by  $\text{H}_4\text{B}$ . Moreover, subsequent conversion of the new heme-oxy intermediate to ferric enzyme is monophasic and occurs at a rate that is equivalent to the rate of L-Arg hydroxylation (or NOHA formation) in the same reaction. Thus, the new intermediate is a catalytically active species whose further reaction is rate-limiting for L-Arg hydroxylation by W188H iNOSoXy.

**The Nature of the Intermediate**—According to Fig. 1, once the heme-dioxy complex (I) is reduced by  $\text{H}_4\text{B}$  there are three transient species that form sequentially: a ferric-peroxo (II), ferric hydroperoxo (III), and a Cpd I-like species (IV). Various methods have been used to create and characterize these species in heme-thiolate enzymes. Reaction of several cytochrome P450 proteins with peroxides or peroxyacids (60–63), or photooxidation of Cpd II (64), has been reported to form a Cpd I-like species. Radiolytic reduction of cytochrome P450<sub>cam</sub> or chloroperoxidase at cryogenic temperature has allowed the observation of ferric-peroxo and ferric-hydroperoxo intermediates (65, 66). These intermediates have also been stabilized in cytochrome P450 by point mutations in the distal heme pocket that may restrict protonation of the ferric-peroxo species (65). Likewise, two groups have observed NOS heme-oxy intermediates in experiments done at cryogenic temperature (67, 68). Radiolytic reduction of a NOS heme-dioxy species formed a ferric-peroxo species (II) as characterized by ENDOR spectroscopy, but no subsequent ferric-hydroperoxo or Cpd I-like species were observed upon further annealing to higher temperature (68). The reaction of NOS with peroxyacids apparently yielded a Cpd I-like species as characterized by EPR (67). A preliminary study has reported a stable heme-oxy intermediate in a nNOS mutant that contains a point substitution in the distal heme pocket (69). Although these studies provide valuable spectroscopic information, the inherent instability of the intermediates and/or limitations of the experimental systems typically prevented concurrent studies being performed on the reactivity or kinetics of the transient intermediates. Nevertheless, the information should help to identify the heme-oxy intermediate that we observe in W188H iNOSoXy. For example, its UV-visible spectrum is most similar to spectra reported either for a ferric-peroxo (II) or a Cpd I-like (IV) intermediate in other heme-thiolate proteins (70–72). It is strikingly similar to the spectrum observed immediately after the cytochrome P450BM3 F87G mutant is reacted with *m*-chloroperoxyben-

zoic acid (70), which the authors assigned to a Cpd I-like species. In contrast, its spectrum differs from that recently reported for the ferric-hydroperoxo intermediate (III) of chloroperoxidase (66).

Cpd I-like species are usually reported to have a significantly reduced Soret absorbance relative to the ferric enzyme. The Soret absorbance that we observe for our new heme-oxy intermediate (peak at 422 nm, Fig. 5) is not as decreased as in some of the canonical examples (60, 63), but is similar to at least one example (70). This may be due in our case to a lingering contribution from the heme-dioxygen spectrum, or perhaps to inherent differences in NOS enzymes relative to other heme-thiolate enzymes, as is already well documented for their heme-dioxy spectra (42, 57). Further experiments are in progress to define the exact nature of the new heme-oxy intermediate in W188H iNOSoxy.

*The Effect of His<sup>188</sup> on the Heme-Thiolate Bond*—The ability of W188H iNOSoxy to stabilize the new heme-oxy intermediate may be related to an effect on the hydrogen bonding between the His<sup>188</sup> side chain and the heme thiolate. Our crystal structure revealed that the N<sup>ε</sup> imidazole atom of the His<sup>188</sup> side chain is within hydrogen bonding distance of the heme thiolate. Hydrogen bonding to the proximal heme ligand has long been considered an important determinant for heme reactivity (see Ref. 73, and references therein). In particular, studies have shown that the reduction potential of the heme is highly dependent on the  $\pi$ -donor strength of the thiolate ligand (74–78). The addition of H-bonds to the thiolate increases the strength of the Fe-S bond, decreases the  $\pi$ -donation of the thiolate, and increases the midpoint reduction potential of the heme (74–77). Our results are consistent with these observations, and suggest that the hydrogen bond between His<sup>188</sup> and the heme-thiolate may be stronger than the one formed in wild-type iNOS by Trp<sup>188</sup>. Because the His imidazole ring has a much lower pK<sub>a</sub> than the indole N-H group of Trp, it is inherently a better H-bond donor. Even at neutral pH it is reasonable to assume that there will be a significant fraction of molecules in which the His<sup>188</sup> side chain will be positively charged, whereas the indole will remain neutral at any given physiological pH. *Ab initio* studies indicate that the analogous NH–O hydrogen bond is slightly stronger for a neutral imidazole than for an indole, but a protonated imidazole makes a much stronger hydrogen bond (79). We do not observe a noticeable shortening of the nitrogen-sulfur distance for the W188H mutant, but it must be noted that the His<sup>188</sup> can hardly get any closer without causing some disruption in the protein backbone.

In model heme-thiolate compounds, changes in midpoint potential ranging from 100 to 200 mV with only one NH–S hydrogen bond have been observed (80–82). Those hydrogen bonds are strong (N–S distances between 2.9 and 3.0 Å (81)) and in heme-thiolate proteins the hydrogen bonds are generally weaker (N–S distances typically between 3.2 and 3.5 Å, with less than optimal angles) and the effects on the potential are proportionally smaller (74–77). Thus, the increased heme midpoint potential of W188H iNOSoxy (+88 mV) could be due in part to the increased strength of the His<sup>188</sup> imidazole NH–S hydrogen bond, relative to Trp<sup>188</sup>. Other aspects to consider include the possibility that the His<sup>188</sup> is protonated and posi-

tively charged, or that the mutation changes heme solvation or the degree of porphyrin bending (40, 83–85) relative to wild-type. These possibilities are under current investigation.

*Mechanistic Insights*—Previous considerations suggest that a Cpd I-like species may be the only intermediate with sufficient power to oxidize a substrate like L-Arg. This would be consistent with studies on cytochrome P450 enzymes that argue a similar hydroxylation would likely involve a Cpd I-like species (86, 87). Thus, if we assume a Cpd I-like species must form in W188H iNOSoxy to generate NOHA, then buildup of the new heme-oxy intermediate and the subsequent slow rate of L-Arg hydroxylation could be due to two circumstances: a poor protonation of the ferric-peroxo and/or ferric-hydroperoxo intermediates (II and III) that would effectively slow formation of the Cpd I-like oxidant, or alternatively, a facile formation of a Cpd I-like species that then builds up because it is too weak an oxidant to react quickly with L-Arg.

In light of these possibilities, how might the higher heme midpoint potential in W188H iNOSoxy impact the formation and/or reactivity of the various heme-oxy species during L-Arg hydroxylation? Precise answers are impossible to infer, because at this point we can only extrapolate based on our measurement of the ferric/ferrous couple, which may or may not be an accurate reflection of the midpoint potentials of the actual reactive heme-oxy species in question. We did observe a 100-fold stabilization of the initial heme-dioxy intermediate (I) in W188H iNOSoxy relative to wild-type when both contained H<sub>2</sub>B to prevent heme-dioxy reduction within the enzyme. A similar stabilization of the heme-dioxy species has been observed in cytochrome P450BM3 mutants that have more positive ferric/ferrous heme midpoint potentials (74, 88). This might be explained by the lower electron density in the heme-thiolate favoring the ferrous-dioxy heme resonance form over the ferric-superoxy heme resonance form (74) (Fig. 1), and thereby inhibiting breakdown into superoxide and ferric heme. The extreme examples would be hemoglobin or myoglobin who have much higher heme midpoint potentials and enable oxygen to remain bound to the ferrous heme for long times without significant autooxidation (89). Interestingly, we found that the heme-dioxy complex in W188H iNOSoxy, despite being more stable, was still reduced by H<sub>4</sub>B in the L-Arg reaction. This contrasts with a cytochrome P450BM3 study, in which the authors suggested that reduction of the heme-dioxy species is likely impaired in the high potential mutants (74). Whether this difference arises from NOS utilizing a closely bound H<sub>4</sub>B cofactor as the reductant instead of a separate subdomain containing reduced FMN cofactor (as does cytochrome P450BM3) is an interesting possibility to explore further.

Regarding protonation of the heme-peroxo and heme-hydroperoxo species (II and III), it is important to realize that there are no protein-based H-bond donors present in the distal heme pocket of NOS (10, 13). Although several proton donors and mechanisms have been proposed for the NOS enzymes, including a structural water molecule, the guanidinium group of L-Arg, and H<sub>4</sub>B (15, 49, 87, 90–92) there is no consensus and none have been experimentally verified. The fact that the W188H mutation is proximal to the heme means it could only have an indirect influence on the distal heme environment

## Stabilization of a Reaction Intermediate in iNOS

where the relevant proton donors are likely to be located. However, there may be precedent for an effect on the protonation steps, because proximal site mutations that alter the heme midpoint potentials of cytochrome P450st and CYP101A1 were suggested to influence protonation of the heme-peroxy species and thus impact Cpd I formation, albeit on the basis of steady-state kinetic measurements (75–77). Similarly, calculations indicate that increased hydrogen bonding to the heme-thiolate should decrease the “push” effect of the sulfur atom and thus may have a negative effect on the heterolytic cleavage of the O–O bond that enables formation of Cpd I (93). It is also possible that the more electropositive heme-thiolate in W188H iNOS<sub>oxy</sub> creates a circumstance where the ferric-peroxy and/or ferric-hydroperoxy species are less basic and therefore less prone to protonation within the distal cavity. Thus, an effect of the W188H mutation on heme-oxy protonation steps is conceivable but the mechanism is unclear at present.

There is little evidence indicating how changes in H-bonding to the heme-thiolate or in heme-thiolate electronegativity would affect the reactivity of a Cpd I-like species. Theoretical calculations predict that formation of stronger hydrogen bonds to the heme-thiolate should increase the reactivity of a Cpd I-like species (17, 18). In manganese peroxidase, proximal mutations that induced  $\pm 80$  mV changes in the ferric/ferrous heme midpoint potential had little effect on the kinetics of its Cpd I reduction, but did slow or speed the rate of its Cpd II reduction (94). On the other hand, no significant correlation was reported between heme midpoint potential and the Cpd I reduction rate in a panel of ascorbate peroxidase mutants (95). Regardless, the possibility that the W188H mutation diminishes the reactivity of a Cpd I-like species remains intriguing and should be explored further.

**Conclusions**—W188H iNOS<sub>oxy</sub> can be a valuable tool to study details of oxygen activation in heme-thiolate enzymes. It is the first example in this family where a proximal site mutation can stabilize a heme-oxy intermediate that forms downstream from the initial heme-dioxy species. This effect has been previously observed only in distal site (65) or other mutants (71). Our results provide an excellent example of how relatively small changes in the proximal heme environment can tune the electronics of the heme-thiolate and in turn modify the processing and/or reactivity of various heme-oxy species. Our findings indicate that a decrease in heme-thiolate electronegativity in iNOS inhibits the formation and/or reactivity of the heme-oxy intermediate that ultimately hydroxylates the substrate L-Arg.

**Acknowledgments**—We thank Profs. Emma Raven, Iliia Denisov, Steven Sligar, and the members of the Stuehr laboratory for helpful discussions. We also thank two anonymous reviewers for helpful comments.

### REFERENCES

- Pfeiffer, S., Mayer, B., and Hemmens, B. (1999) *Angew. Chem. Int. Ed.* **38**, 1714–1731
- Guzik, T. J., Korbut, R., and Adamek-Guzik, T. (2003) *J. Physiol. Pharmacol.* **54**, 469–487
- Yun, H. Y., Dawson, V. L., and Dawson, T. M. (1997) *Mol. Psychiatry* **2**, 300–310
- Barbato, J. E., and Tzeng, E. (2004) *J. Vasc. Surg.* **40**, 187–193
- Alderton, W. K., Cooper, C. E., and Knowles, R. G. (2001) *Biochem. J.* **357**, 593–615
- Stuehr, D. J. (1999) *Biochim. Biophys. Acta* **1411**, 217–230
- Bredt, D. S., Hwang, P. M., Glatt, C. E., Lowenstein, C., Reed, R. R., and Snyder, S. H. (1991) *Nature* **351**, 714–718
- Wang, M., Roberts, D. L., Paschke, R., Shea, T. M., Masters, B. S., and Kim, J. J. (1997) *Proc. Natl. Acad. Sci. U. S. A.* **94**, 8411–8416
- Garcin, E. D., Bruns, C. M., Lloyd, S. J., Hosfield, D. J., Tiso, M., Gachhui, R., Stuehr, D. J., Tainer, J. A., and Getzoff, E. D. (2004) *J. Biol. Chem.* **279**, 37918–37927
- Crane, B. R., Arvai, A. S., Ghosh, D. K., Wu, C., Getzoff, E. D., Stuehr, D. J., and Tainer, J. A. (1998) *Science* **279**, 2121–2126
- Raman, C. S., Li, H., Martasek, P., Kral, V., Masters, B. S., and Poulos, T. L. (1998) *Cell* **95**, 939–950
- Mansuy, D., and Renaud, J. P. (1995) in *Cytochrome P450: Structure, Mechanism, and Biochemistry* (Ortiz de Montellano, P. R., ed) pp. 537–574, Plenum Press, New York
- Crane, B. R., Arvai, A. S., Gachhui, R., Wu, C., Ghosh, D. K., Getzoff, E. D., Stuehr, D. J., and Tainer, J. A. (1997) *Science* **278**, 425–431
- Fischmann, T. O., Hruza, A., Niu, X. D., Fossetta, J. D., Lunn, C. A., Dolphin, E., Prongay, A. J., Reichert, P., Lundell, D. J., Narula, S. K., and Weber, P. C. (1999) *Nat. Struct. Biol.* **6**, 233–242
- Li, H., and Poulos, T. L. (2005) *J. Inorg. Biochem.* **99**, 293–305
- Ost, T. W., Miles, C. S., Munro, A. W., Murdoch, J., Reid, G. A., and Chapman, S. K. (2001) *Biochemistry* **40**, 13421–13429
- Poulos, T. L. (2005) *Phil. Trans. R. Soc. A* **363**, 793–806
- Ogliaro, F., Cohen, S., de Visser, S. P., and Shaik, S. (2000) *J. Am. Chem. Soc.* **122**, 12892–12893
- Adak, S., and Stuehr, D. J. (2001) *J. Inorg. Biochem.* **83**, 301–308
- Adak, S., Wang, Q., and Stuehr, D. J. (2000) *J. Biol. Chem.* **275**, 17434–17439
- Adak, S., Crooks, C., Wang, Q., Crane, B. R., Tainer, J. A., Getzoff, E. D., and Stuehr, D. J. (1999) *J. Biol. Chem.* **274**, 26907–26911
- Panda, K., Haque, M. M., Garcin-Hosfield, E. D., Durra, D., Getzoff, E. D., and Stuehr, D. J. (2006) *J. Biol. Chem.* **281**, 36819–36827
- Konas, D. W., Takaya, N., Sharma, M., and Stuehr, D. J. (2006) *Biochemistry* **45**, 12596–12609
- Ghosh, D. K., Wu, C., Pitters, E., Moloney, M., Werner, E. R., Mayer, B., and Stuehr, D. J. (1997) *Biochemistry* **36**, 10609–10619
- Wu, C., Zhang, J., Abu-Soud, H., Ghosh, D. K., and Stuehr, D. J. (1996) *Biochem. Biophys. Res. Commun.* **222**, 439–444
- Stuehr, D. J., and Ikeda-Saito, M. (1992) *J. Biol. Chem.* **267**, 20547–20550
- Ilagan, R. P., Tiso, M., Konas, D. W., Hemann, C., Durra, D., Hille, R., and Stuehr, D. J. (2008) *J. Biol. Chem.* **283**, 19603–19615
- Pflugrath, J. W. (1999) *Acta Crystallogr. Sect. D Biol. Crystallogr.* **55**, 1718–1725
- McCoy, A. J., Grosse-Kunstleve, R. W., Adams, P. D., Winn, M. D., Storoni, L. C., and Read, R. J. (2007) *J. Appl. Crystallogr.* **40**, 658–674
- Emsley, P., and Cowtan, K. (2004) *Acta Crystallogr. Sect. D Biol. Crystallogr.* **60**, 2126–2132
- Adams, P. D., Grosse-Kunstleve, R. W., Hung, L. W., Ioerger, T. R., McCoy, A. J., Moriarty, N. W., Read, R. J., Sacchettini, J. C., Sauter, N. K., and Terwilliger, T. C. (2002) *Acta Crystallogr. Sect. D Biol. Crystallogr.* **58**, 1948–1954
- McMillan, K., and Masters, B. S. (1993) *Biochemistry* **32**, 9875–9880
- Wang, Z. Q., Wei, C. C., and Stuehr, D. J. (2002) *J. Biol. Chem.* **277**, 12830–12837
- Wei, C. C., Wang, Z. Q., Wang, Q., Meade, A. L., Hemann, C., Hille, R., and Stuehr, D. J. (2001) *J. Biol. Chem.* **276**, 315–319
- Wei, C. C., Wang, Z. Q., Tejero, J., Yang, Y. P., Hemann, C., Hille, R., and Stuehr, D. J. (2008) *J. Biol. Chem.* **283**, 11734–11742
- Abu-Soud, H. M., Presta, A., Mayer, B., and Stuehr, D. J. (1997) *Biochemistry* **36**, 10811–10816
- Boggs, S., Huang, L., and Stuehr, D. J. (2000) *Biochemistry* **39**, 2332–2339
- Wilson, D. J., and Rafferty, S. P. (2001) *Biochem. Biophys. Res. Commun.* **287**, 126–129

39. Presta, A., Siddhanta, U., Wu, C., Sennequier, N., Huang, L., Abu-Soud, H. M., Erzurum, S., and Stuehr, D. J. (1998) *Biochemistry* **37**, 298–310
40. Presta, A., Weber-Main, A. M., Stankovich, M. T., and Stuehr, D. (1998) *J. Am. Chem. Soc.* **120**, 9460–9465
41. Gao, Y. T., Smith, S. M., Weinberg, J. B., Montgomery, H. J., Newman, E., Guillemette, J. G., Ghosh, D. K., Roman, L. J., Martasek, P., and Salerno, J. C. (2004) *J. Biol. Chem.* **279**, 18759–18766
42. Wei, C. C., Crane, B. R., and Stuehr, D. J. (2003) *Chem. Rev.* **103**, 2365–2383
43. Hurshman, A. R., Krebs, C., Edmondson, D. E., Huynh, B. H., and Marletta, M. A. (1999) *Biochemistry* **38**, 15689–15696
44. Bec, N., Gorren, A. C., Voelker, C., Mayer, B., and Lange, R. (1998) *J. Biol. Chem.* **273**, 13502–13508
45. Sligar, S. G., Makris, T. M., and Denisov, I. G. (2005) *Biochem. Biophys. Res. Commun.* **338**, 346–354
46. Makris, T. M., von Koenig, K., Schlichting, I., and Sligar, S. G. (2006) *J. Inorg. Biochem.* **100**, 507–518
47. Shaik, S., Kumar, D., de Visser, S. P., Altun, A., and Thiel, W. (2005) *Chem. Rev.* **105**, 2279–2328
48. Sono, M., Roach, M. P., Coulter, E. D., and Dawson, J. H. (1996) *Chem. Rev.* **96**, 2841–2888
49. Zhu, Y., and Silverman, R. B. (2008) *Biochemistry* **47**, 2231–2243
50. Gorren, A. C. F., and Mayer, B. (2007) *Biochim. Biophys. Acta* **1770**, 432–445
51. Stuehr, D. J., Santolini, J., Wang, Z. Q., Wei, C. C., and Adak, S. (2004) *J. Biol. Chem.* **279**, 36167–36170
52. Abu-Soud, H. M., Gachhui, R., Raushel, F. M., and Stuehr, D. J. (1997) *J. Biol. Chem.* **272**, 17349–17353
53. Berka, V., Wang, L. H., and Tsai, A. L. (2008) *Biochemistry* **47**, 405–420
54. Marchal, S., Gorren, A. C., Sorlie, M., Andersson, K. K., Mayer, B., and Lange, R. (2004) *J. Biol. Chem.* **279**, 19824–19831
55. Wang, Z. Q., Wei, C. C., Ghosh, S., Meade, A. L., Hemann, C., Hille, R., and Stuehr, D. J. (2001) *Biochemistry* **40**, 12819–12825
56. Couture, M., Stuehr, D. J., and Rousseau, D. L. (2000) *J. Biol. Chem.* **275**, 3201–3205
57. Ledbetter, A. P., McMillan, K., Roman, L. J., Masters, B. S., Dawson, J. H., and Sono, M. (1999) *Biochemistry* **38**, 8014–8021
58. Sono, M., Stuehr, D. J., Ikeda-Saito, M., and Dawson, J. H. (1995) *J. Biol. Chem.* **270**, 19943–19948
59. Wei, C. C., Wang, Z. Q., Arvai, A. S., Hemann, C., Hille, R., Getzoff, E. D., and Stuehr, D. J. (2003) *Biochemistry* **42**, 1969–1977
60. Egawa, T., Shimada, H., and Ishimura, Y. (1994) *Biochem. Biophys. Res. Commun.* **201**, 1464–1469
61. Schunemann, V., Jung, C., Trautwein, A. X., Mandon, D., and Weiss, R. (2000) *FEBS Lett.* **479**, 149–154
62. Spolitak, T., Dawson, J. H., and Ballou, D. P. (2005) *J. Biol. Chem.* **280**, 20300–20309
63. Kellner, D. G., Hung, S. C., Weiss, K. E., and Sligar, S. G. (2002) *J. Biol. Chem.* **277**, 9641–9644
64. Newcomb, M., Zhang, R., Chandrasena, R. E., Halgrimson, J. A., Horner, J. H., Makris, T. M., and Sligar, S. G. (2006) *J. Am. Chem. Soc.* **128**, 4580–4581
65. Davydov, R., Makris, T. M., Kofman, V., Werst, D. E., Sligar, S. G., and Hoffman, B. M. (2001) *J. Am. Chem. Soc.* **123**, 1403–1415
66. Denisov, I. G., Dawson, J. H., Hager, L. P., and Sligar, S. G. (2007) *Biochem. Biophys. Res. Commun.* **363**, 954–958
67. Jung, C., Lenzian, F., Schunemann, V., Richter, M., Bottger, L. H., Trautwein, A. X., Contzen, J., Galander, M., Ghosh, D. K., and Barra, A. L. (2005) *Magn. Reson. Chem.* **43**, S84–S95
68. Davydov, R., Ledbetter-Rogers, A., Martasek, P., Larukhin, M., Sono, M., Dawson, J. H., Masters, B. S., and Hoffman, B. M. (2002) *Biochemistry* **41**, 10375–10381
69. Papale, D., Miles, C. C., and Daff, S. (2007) *J. Biol. Inorg. Chem.* **12**, S199
70. Benson, D. E., Suslick, K. S., and Sligar, S. G. (1997) *Biochemistry* **36**, 5104–5107
71. Raner, G. M., Thompson, J. I., Haddy, A., Tangham, V., Bynum, N., Ramachandra, R. G., Ballou, D. P., and Dawson, J. H. (2006) *J. Inorg. Biochem.* **100**, 2045–2053
72. Lad, L., Mewies, M., and Raven, E. L. (2002) *Biochemistry* **41**, 13774–13781
73. Poulos, T. L. (1996) *J. Biol. Inorg. Chem.* **1**, 356–359
74. Ost, T. W., Clark, J., Mowat, C. G., Miles, C. S., Walkinshaw, M. D., Reid, G. A., Chapman, S. K., and Daff, S. (2003) *J. Am. Chem. Soc.* **125**, 15010–15020
75. Yoshioka, S., Takahashi, S., Ishimori, K., and Morishima, I. (2000) *J. Inorg. Biochem.* **81**, 141–151
76. Yoshioka, S., Tosha, T., Takahashi, S., Ishimori, K., Hori, H., and Morishima, I. (2002) *J. Am. Chem. Soc.* **124**, 14571–14579
77. Matsumura, H., Wakatabi, M., Omi, S., Ohtaki, A., Nakamura, N., Yohda, M., and Ohno, H. (2008) *Biochemistry* **47**, 4834–4842
78. Glascock, M. C., Ballou, D. P., and Dawson, J. H. (2005) *J. Biol. Chem.* **280**, 42134–42141
79. Scheiner, S., Kar, T., and Pattanayak, J. (2002) *J. Am. Chem. Soc.* **124**, 13257–13264
80. Ueyama, N., Yamada, Y., Okamura, T. T., Kimura, S., and Nakamura, A. (1996) *Inorg. Chem.* **35**, 6473–6484
81. Ueyama, N., Nishikawa, N., Yamada, Y., Okamura, T., Oka, S., Sakurai, H., and Nakamura, A. (1998) *Inorg. Chem.* **37**, 2415–2421
82. Suzuki, N., Higuchi, T., Urano, Y., Kikuchi, K., Uekusa, H., Ohashi, Y., Uchida, T., Kitagawa, T., and Nagano, T. (1999) *J. Am. Chem. Soc.* **121**, 11571–11572
83. Voigt, P., and Knapp, E. W. (2003) *J. Biol. Chem.* **278**, 51993–52001
84. Song, Y., Mao, J., and Gunner, M. R. (2006) *Biochemistry* **45**, 7949–7958
85. Li, D., Stuehr, D. J., Yeh, S. R., and Rousseau, D. L. (2004) *J. Biol. Chem.* **279**, 26489–26499
86. Groves, J. T., and Wang, C. C. (2000) *Curr. Opin. Chem. Biol.* **4**, 687–695
87. Cho, K. B., Derat, E., and Shaik, S. (2007) *J. Am. Chem. Soc.* **129**, 3182–3188
88. Clark, J. P., Miles, C. S., Mowat, C. G., Walkinshaw, M. D., Reid, G. A., Daff, S. N., and Chapman, S. K. (2006) *J. Inorg. Biochem.* **100**, 1075–1090
89. Shikama, K. (2006) *Prog. Biophys. Mol. Biol.* **91**, 83–162
90. Li, H., Raman, C. S., Martasek, P., Masters, B. S., and Poulos, T. L. (2001) *Biochemistry* **40**, 5399–5406
91. Sorlie, M., Gorren, A. C., Marchal, S., Shimizu, T., Lange, R., Andersson, K. K., and Mayer, B. (2003) *J. Biol. Chem.* **278**, 48602–48610
92. de Visser, S. P., and Tan, L. S. (2008) *J. Am. Chem. Soc.*, **130**, 12961–12974
93. Ogliaro, F., de Visser, S. P., and Shaik, S. (2002) *J. Inorg. Biochem.* **91**, 554–567
94. Whitwam, R. E., Koduri, R. S., Natan, M., and Tien, M. (1999) *Biochemistry* **38**, 9608–9616
95. Efimov, I., Papadopoulou, N. D., McLean, K. J., Badyal, S. K., Macdonald, I. K., Munro, A. W., Moody, P. C., and Raven, E. L. (2007) *Biochemistry* **46**, 8017–8023
96. DeLano, W. (2002) *The PyMol Molecular Graphics System*, DeLano Scientific, Palo Alto, CA